From Concept to Application: Machine Learning for Near-Real-Time River Ice Breakup Prediction Using SAR and Meteorological Data

Maria Yulmetova, Pradeep Bobby, Michael Lynch, Ian Turnbull

Centre for Cold Ocean Resources Engineering (C-CORE), 1 Morrissey Rd, St. John's, NL, Canada
(maria.yulmetova; pradeep.bobby; michael.lynch; ian.turnbull)@c-core.ca

Keywords: River ice, Breakup prediction, Synthetic Aperture Radar, Machine learning.

Abstract

Accurate, reliable, and early-warning forecasts of river ice breakup are essential for flood risk mitigation and public safety, particularly in relation to river transportation and ice road operations. Synthetic Aperture Radar (SAR) satellite imagery has been widely utilized for monitoring river ice conditions due to its sensitivity to surface roughness and dielectric properties. This study advances traditional SAR applications and, to our knowledge, presents the first model that directly incorporates SAR data as input within a machine learning (ML) framework for river ice breakup prediction. The method leverages the correlation between SAR backscatter dynamics and the onset of surface melt. The model was evaluated using leave-one-out cross-validation, achieving an overall accuracy of 92%, an F1-score of 0.91, a Kappa coefficient of 0.84, and a mean absolute error (MAE) of less than 6 days for both the two- and three-week forecasts. The algorithm was also implemented in near-real-time operational settings, demonstrating strong performance with MAE values ranging from zero to four days across different river segments. The approach was further tested on an independent site, where it maintained robust predictive skill. The newly developed method shows strong potential for two- and three-week forecasting of river ice breakup, offering a scalable, cost-effective, and operationally viable tool for management and early warning applications.

1. Introduction

Forecasting river ice breakup is essential for public safety, environmental monitoring, and operational decision-making in northern regions.

First, river ice breakup events can lead to the formation of ice jams, which in turn may cause severe flooding. Such events pose significant threats to nearby communities, infrastructure, and ecosystems (Chaouch et al., 2014). Reliable breakup forecasts help authorities to better assess potential risks and issue early warnings.

Second, breakup forecasting plays a key role in the management of seasonal transportation networks in northern and remote regions. In Canada, the ice road network extends over approximately 10,000 km (Gädeke et al., 2021). For many northern communities, these routes represent the only overland means of transportation and delivery of essential goods and supplies. Therefore, continuous monitoring of ice road conditions, combined with accurate and advanced forecasting of ice breakup, is critical for the safe use of these roads.

In addition, historical records of river ice breakup serve as valuable climate proxies. As global temperatures continue to rise, shifts in the timing and duration of ice breakup have been increasingly observed, providing important insights into both regional and global climate trends (Magnuson et al., 2000; Mullan et al., 2017).

Although numerous modeling approaches have been proposed to predict the timing of river ice breakup, most of these models are highly site-specific and therefore difficult to generalize, as they often rely on location-specific data, such as in situ measurements of ice thickness, temperature, or ice composition.

Collecting these data requires extensive fieldwork, which is costly and logistically complex. For northern rivers, obtaining field measurements is especially challenging due to their remote and often inaccessible locations. As a result, both the temporal frequency and spatial coverage of in situ observations are sporadic, limited, and inconsistent. Consequently, a major limitation frequently noted in the literature is the lack of consistent and continuous observational data, which constrains the development of generalized predictive models (Rokaya et al., 2020).

The increasing availability of high- and medium-resolution satellite data provides a promising alternative, offering consistent, wide-area, and temporally frequent measurements. The availability of satellite data, particularly SAR observations, has increased significantly in recent years. In addition to Sentinel-1A, which has been operational since April 2014, Sentinel-1C was launched on 5 December 2024, and Sentinel-1D is scheduled for launch at the end of 2025, further expanding the temporal coverage. The launch of the three Radarsat Constellation Mission (RCM) satellites in 2019 has significantly increased the availability of SAR data over Canada. This opened new opportunities to efficiently collect large datasets for machine learning applications, including the development of predictive models for ice breakup.

SAR imagery has proven to be a reliable source for monitoring river ice conditions (Sobiech & Dierking, 2013; van der Sanden et al., 2021). Compared to optical sensors, SAR offers the advantage of penetrating cloud cover and operating independently of solar illumination, enabling all-weather, day-and-night observations. This is particularly advantageous for monitoring dynamic processes such as river ice breakup, which often coincides with rising air temperatures that lead to increased cloud cover, fog, and reduced visibility.

Furthermore, SAR signals can penetrate dry snow layers and provide information about the dielectric properties of the surface (Solberg et al., 2010). The penetration depth depends on signal frequency, wavelength, polarization, and snowpack

This contribution has been peer-reviewed. The double-blind peer-review was conducted on the basis of the full paper.
https://doi.org/10.5194/isprs-annals-XI-M-1-2026-79-2026

characteristics, such as grain size, density, liquid water content, surface roughness, and snow depth (Bamler & Hartl, 1998; Brangers et al., 2024). Numerous studies have leveraged these unique sensing capabilities of SAR to investigate melting processes on ice sheets, sea ice, and mountain regions (Eckerstorfer & Malnes, 2015; Jutila & Haas, 2025; Lund et al., 2022; Snapir et al., 2019). However, to date, the use of SAR to detect surface melt onset in river systems and its integration into predictive modeling remains largely unexplored.

This research proposes an approach that leverages the correlation between SAR backscatter dynamics and the onset of river ice surface melt to develop a ML model. By capturing the early signals of surface thaw, the proposed methodology aims to provide a scalable and cost-effective solution for forecasting river ice breakup in near-real-time settings.

2. Study Area

The area of interest for this study is the lower section of the Churchill River, located in Newfoundland and Labrador, Canada. The Churchill River, with a total length of approximately 856 km, is the longest river in Atlantic Canada. It originates from the Smallwood Reservoir and flows eastward before discharging into the Atlantic Ocean through Lake Melville.

This research focuses specifically on the river section located between the Muskrat Falls Hydroelectric Dam and the river's outlet at Lake Melville (Figure 1). This section of the Churchill River is monitored as it is prone to ice jams that can further lead to flooding. Of particular concern is the small community of Mud Lake, situated along the Mud Lake channel that connects to the Churchill River. This community is highly vulnerable to flooding events associated with ice jams forming along the lower Churchill River.

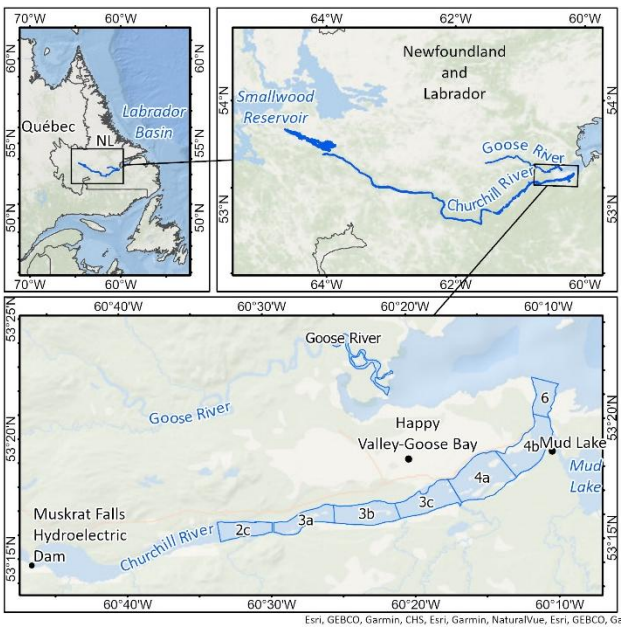

Figure 1. Segments over the Churchill River and Goose River analysed in this project.

A notable event occurred during the spring breakup of 2017, when broken ice accumulated within segments 4b and 6, obstructing the flow from Mud Lake. This ice jam caused a rapid rise in water levels in the Mud Lake channel, leading to the inundation of the Mud Lake community. Residents were evacuated by helicopter to Happy Valley–Goose Bay. Severe flooding was also reported along Mud Lake Road on the western side of the Churchill River. This event caused extensive property damage and highlighted the need for improved monitoring and flood warning and alert system (ECC NL, n.d.).

3. Data

For this project, data from RADARSAT Constellation Mission (RCM), a side-looking radar system operating at C-band, were used. HH polarized Ground Range Detected images obtained in the Scanning Synthetic Aperture Radar (ScanSAR) system with 30 m resolution mode acquired over the Churchill River area from 2020 to 2025 were obtained from the Earth Observation Data Management System (Natural Resources Canada, n.d.-b).

Ice classification products developed by C-CORE were made available to the authors for this study. C-CORE has delivered a near-real-time operational river ice monitoring service for the Churchill River since 2008 to support river ice modeling and flood forecasting (C-CORE, 2024; Lynch et al., 2021). RCM and Sentinel-1 SAR imageries are used to classify river ice into four categories: open water, water on ice or wet ice, non-consolidated ice, and consolidated ice. This dataset served as a key data source for identifying and characterizing river ice conditions throughout the ice season. The open water polygons extracted from these classification products were analyzed through a temporal assessment to quantify seasonal variations in open water extent as well as to define breakup dates.

In addition, other freely available data were used for visual assessment to confirm the breakup dates for model training and validation. These data include Sentinel-1 and Sentinel-2 images obtained from Copernicus Data Space Ecosystem (CDSE, 2025) and Landsat-8/9 images acquired from the United States Geological Survey (USGS, 2025).

Historical 2-meter hourly temperature data were extracted from ERA5 data, the fifth generation of the global atmospheric reanalysis produced by the Copernicus Climate Change Service at the European Centre for Medium-Range Weather Forecasts (ECMWF) (CCCS, 2023).

Lastly, imagery acquired from webcams installed on near-real-time stations (Department of Environment and Climate Change, 2025) along the Churchill River was used as an auxiliary data source to validate the information derived from satellite observations. These ground-based visual records provided valuable and independent confirmation of surface conditions, such as thawing and the progression of ice breakup.

4. Methods

4.1 Proposed Concept

Synthetic Aperture Radar uses backscattered electromagnetic energy to infer physical and dielectric properties of ground targets. SAR signals can penetrate the snow surface as well as provide information on the dielectric properties of snow and ice, supporting detection of surface melt and ice condition assessment (Hoppinen et al., 2024; Solberg et al., 2010). As melting begins, changing dielectric properties reduce penetration depth and alter scattering mechanisms. Increasing liquid water content leads to decreased backscatter (Tsai et al., 2019). A time series of SAR backscatter observations can therefore be used to identify the start of the ice/snow surface thawing process, which is one of the key indicators of an upcoming ice breakup as it directly affects

This contribution has been peer-reviewed. The double-blind peer-review was conducted on the basis of the full paper.
https://doi.org/10.5194/isprs-annals-XI-M-1-2026-79-2026 | © Author(s) 2026. CC BY 4.0 License.

ice stability (Johnson et al., 2020; Ohmura, 2001; Scambos et al., 2000).

Figure 2 illustrates the time series of the SAR backscatter coefficient dynamics extracted from RCM images over Churchill River, segment 3. High variability of backscatter during the period of November-December can be observed, indicating the early stage of the ice season, when ice is either absent or just beginning to form. Starting from mid-January, the backscatter values become stable and higher, reflecting that the river surface is frozen.

An interesting shift can be observed in mid-March, when the backscatter coefficient dropped abruptly for a short period. The drop in backscatter likely resulted from surface melting caused by the warm conditions. Shortly afterward, the backscatter values recovered, suggesting that the surface refroze once temperatures declined.

At the beginning of April, a significant drop in backscatter values was observed; however, this time the values remained low for the rest of the season. It is proposed that this marked decline indicates the onset of surface melting, serving as an early indicator of the forthcoming breakup. Web camera images acquired on April 11 and April 14 also show partial surface thaw, further supporting this interpretation. At this stage, the ice surface was melting, but ice cover was still present. The actual breakup occurred a couple of weeks later. Open-water areas were visible on the web camera images after April 27. We can also observe an increase in noise in the backscatter response from the end of April, which likely reflects the presence of moving ice and/or wind effects on the water surface.

This observed correlation between SAR backscatter response and surface melting led us to propose that the onset of surface thawing can be detected in advance of the actual river ice breakup. Identifying this early signal provides an opportunity to improve the forecasting of breakup events. Based on this concept, we developed and evaluated a ML model designed to predict river ice breakup. The model was trained, validated, and subsequently implemented in near-real time during the 2024-2025 ice season.

4.2 Breakup Definition

It is important to note that the definition of breakup date varies in the literature depending on the application, water body characteristics, geographic location, observation methods, and other factors. Historical efforts to standardize breakup definitions in Canada revealed significant inconsistencies, ranging from the first signs of melting to the complete disappearance of ice (Catchpole & Moodie, 1974; Liston & Hall, 1995). Today, many researchers define ice breakup as a complex sequence of events that may extend over a prolonged period and last several weeks. (Beltaos, 2014; Magnuson et al., 2000; Muhammad et al., 2016; van der Sanden et al., 2021). Moreover, the breakup process can be temporarily paused or even reversed. This makes it difficult to define and pinpoint these moments in time, hindering the establishment of a standardized definition. Therefore, we considered it essential to explicitly define the breakup criterion applied in this study and to outline the reasoning for adopting this definition.

During visual analysis of satellite imagery over the Churchill River, it was observed that multiple breakup phases could occur simultaneously in different sections of the river. This frequently resulted in scenarios where open water appears in isolated areas while ice remains in between. To account for this spatial variability, the river was divided into smaller segments, and breakup dates were determined for each segment individually.

The timing and intensity of these events also varied between river segments and across seasons, introducing additional complexity to the breakup definition. However, it was also concluded that the initial appearance of open water had limited relevance for flood risk assessment, as it did not necessarily indicate significant ice weakening. Therefore, in this project, the breakup date was defined as the point when the open-water area exhibited a rapid increase. All subsequent analyses were based on this definition.

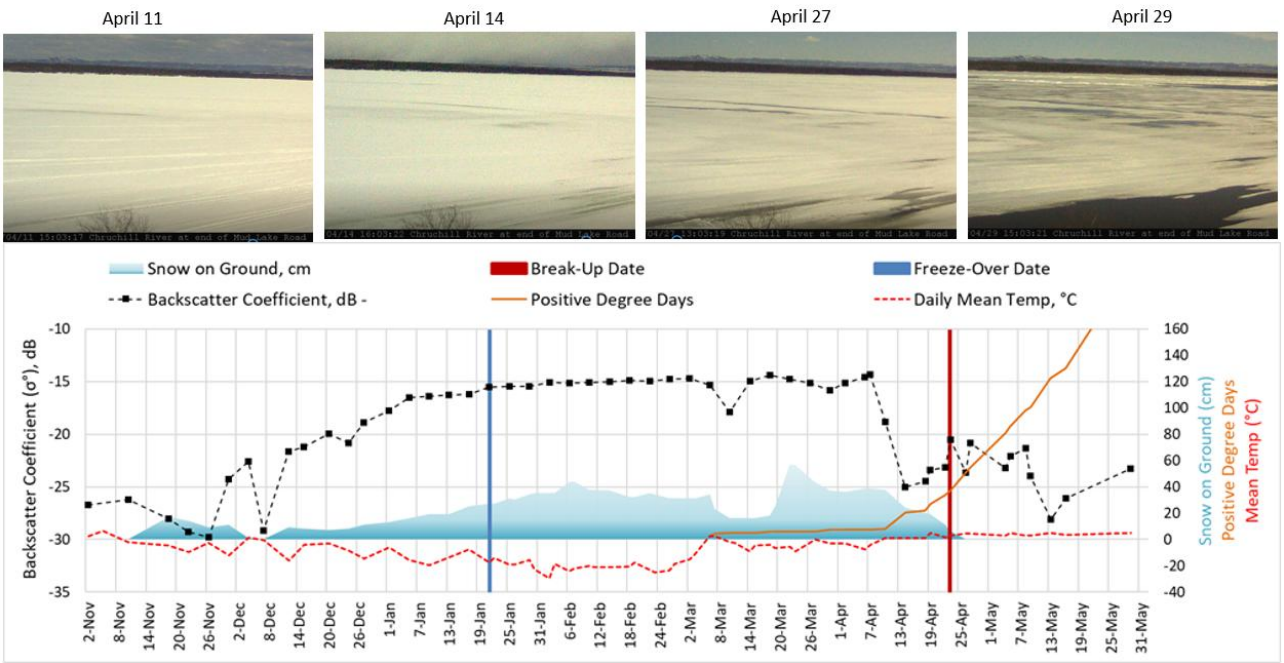

Figure 2. Time series of SAR backscatter observations over Churchill River Segment 3 during the 2022–2023 season, along with webcam images.

This contribution has been peer-reviewed. The double-blind peer-review was conducted on the basis of the full paper.
https://doi.org/10.5194/isprs-annals-XI-M-1-2026-79-2026 | © Author(s) 2026. CC BY 4.0 License.

4.3 Model Development

First, the river was divided into several segments to generate breakup forecasts for each section. However, it is important to consider that rivers are complex systems: in some years, certain areas may remain ice-free throughout the season, resulting in persistent open water. These open-water areas can vary in size and location from year to year, which complicates the determination of the breakup date. Examples of this variability are shown in Figure 3, illustrating that both the extent and location of persistent open water change annually. For instance, in 2022, part of segment 3a remained open while the rest of the river was frozen. In contrast, during the 2024 season, segment 3a was almost entirely frozen, whereas open water appeared in other segments.

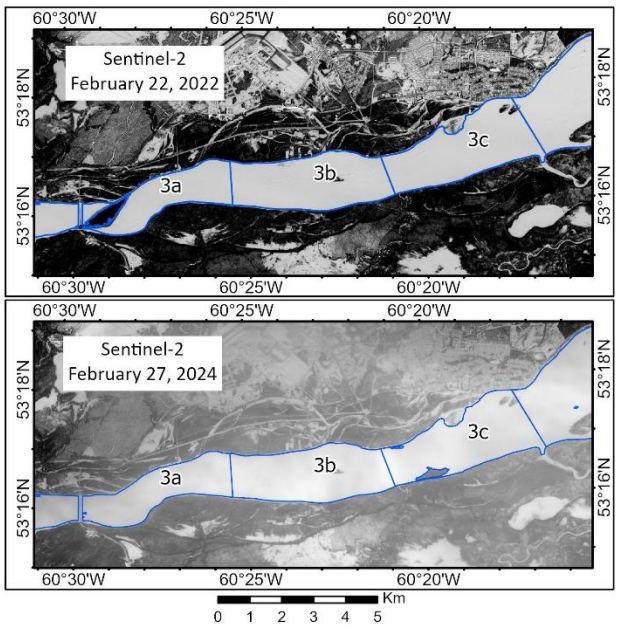

Figure 3.Year-to-year changes in the extent and distribution of open water remaining unfrozen during the season.

To address this challenge, the polygons were defined for each year separately by excluding areas of open water that persist during the peak of the ice season. For that, the areas of open water were extracted from classification products obtained from C-CORE and were analyzed as a time series to determine the date with the least amount of water present. The areas of open water present on these dates were excluded. This ensures a more accurate determination of the ice breakup date by focusing only on regions that were frozen during a specific year.

Second, labels were derived from observed breakup dates. For each polygon, the breakup date was defined as the moment of a rapid expansion in the extent of open water, identified through temporal analysis of open water area derived from C-CORE's classification products. The results were additionally validated through visual inspection of optical imagery.

Then, the predictor variables, comprising SAR backscatter and positive degree days (PDD), were derived. The backscatter coefficient was extracted from RCM SAR images following radiometric calibration, the Range Doppler orthorectification (Small & Schubert, 2008) using the Canadian Digital Elevation Model (CDEM)(Natural Resources Canada, n.d.-a), and Lee filtering (Lee, 1980) with a kernel size of 3 by 3. The ERA5 2-meter hourly temperature estimates were extracted and interpolated for each segment of interest. These data were used to calculate PDD for each segment as the cumulative sum of daily average temperatures above 0°C starting from February.

Next, a neural network (NN) multilayer perceptron (MLP) classifier was trained. Each input sample consisted of SAR backscatter and PDD values corresponding to a given forecast horizon (2 and 3 weeks) for a specific river segment. The target label indicated whether a breakup occurs within the specified forecast horizon for that segment. On average, around 80 data points per segment were available for training. The output is the probability of breakup occurring within the forecast window. The network was trained using a stochastic gradient descent optimizer with adaptive learning, allowing a maximum of 1000 training iterations. The hyperbolic tangent function served as the activation function. The MLP architecture consisted of two hidden layers with 50 and 10 neurons, respectively, and a fixed random seed of 1 was used to ensure reproducibility of results.

Finally, Leave-One-Out Cross-Validation (LOOCV) was used to evaluate model performance due to the small size of our dataset. During this validation method, the model was repeatedly trained multiple times, each time leaving out one data point as a test case while using all remaining points for training. This approach ensured that every sample was tested on a model that had never seen it before, providing an unbiased estimate of model accuracy. Overall Accuracy (OA), F1-score, and Cohen's Kappa were computed from the LOOCV results to allow a robust and fair evaluation.

It must also be noticed that our training dataset consists of data collected from March to May; however, it is known that the probability of breakup is very low in early March and, conversely, very high in late May. Therefore, relying solely on standard metrics like OA, F1-score, and Kappa coefficient may not provide a reliable measure of performance. Moreover, these traditional metrics can be difficult to interpret in practical terms, as they do not show how many days the model is likely to predict the breakup correctly.

To address this limitation, along with traditional metrics, we also calculated the mean absolute error (MAE) to quantify the average deviation (in days) between the predicted and actual breakup dates. To implement this, the predicted probabilities for each data point were first generated using the LOOCV approach. Then, for each year, the dates at which the predicted probability reached 50% were determined using linear interpolation. Finally, the differences between the 50% probability dates and the actual breakup dates were calculated for each segment. This approach allowed us to quantify the temporal accuracy of our model.

4.4 Model Operationalization

The developed algorithm was run in a near-real-time operational setting during the 2024-2025 river ice season. The model was triggered each time a new RCM image became available.

The model used SAR backscatter and PDD as input data to predict the likelihood of a breakup event occurring within a specific forecast period. These forecasts were subsequently delivered to the client to support operational management.

The operational performances of the two-week and three-week forecast models were assessed after the season. Similarly, as described in section 4.3, MAEs were calculated between the

dates when the predicted probability reached 50% and the corresponding observed breakup dates.

4.5 Model Validation on an Independent Site

We trained and evaluated the developed processing chain on a separate site, over the western section of Goose River, to assess site-specific performance. This analysis was conducted independently of the original model. For consistency and comparability, the same performance metrics employed during the initial model evaluation, including MAE, OA, F1-score, and Cohen's Kappa, were applied to quantify the algorithm's performance at the new site.

5. Results

5.1 Model Evaluation Results

As described in Section 4, the river was segmented into defined polygons, created separately for each year by excluding areas of open water that persisted during the peak of the ice season. These areas were identified through time series analysis of open-water extent, with the minimum extents observed on February 22, 2021; February 25, 2022; February 27, 2023; and February 25, 2024. From these polygons, backscatter coefficient values, temperature-derived PDD, and observed breakup dates were extracted and used to train and validate segment-specific NN MLP models for river ice breakup prediction.

Table 1 summarizes the evaluation metrics derived from LOOCV. In addition, the MAE was calculated to quantify the average deviation (in days) between the predicted and actual breakup dates. For each year, the difference between the date when the predicted probability reached 50% and the observed breakup date was computed, and the averages of these differences for each segment are also presented in Table 1. It also includes the results of models applied to the western part of the Goose River for spatial transferability assessment.

Overall, both the 2-week and 3-week forecast models performed comparably, with only minimal differences in evaluation metrics. The MAE values indicate that, on average, the predicted breakup dates deviated from the observed dates by less than six days, with standard deviations of less than four days. The OA values and F1-scores (both higher than 0.9) further confirm high classification performance, while the Cohen's Kappa coefficient of 0.84 reflects a substantial agreement between the predicted and actual class (Landis & Koch, 1977).

Interestingly, both models exhibited the lowest OA and Kappa values for segment 3c. The underlying reasons for this reduced performance are not immediately clear. It may be suggested that the location of segment 3c in the central part of the study area may contribute to its variability: upstream segments tend to melt earlier due to the influence of deeper bathymetry and the presence of a dam, while downstream segments are affected by inflow from the Mud lake channel, which typically breaks up first. Further investigation is needed to better understand these spatial differences and to improve model performance in this transition zone.

The developed algorithm was also implemented over the western section of the Goose River to assess site-specific performance. The results indicated that the model's performance varied depending on the prediction horizon.

For the two-week horizon, the classification metrics show only a slight decrease compared to the original site. The MAE over the Goose River was slightly higher than the average MAE across all the Churchill River segments, indicating a minor reduction in predictive accuracy. However, the substantially higher standard deviation (5.12 versus 3.46) demonstrated greater variability in prediction errors. This suggests that the two-week model can be applied to other rivers, but variability in error should be monitored.

In contrast, the three-week model exhibited a noticeable decline in performance across all metrics when applied to the new site. The significant reductions in all evaluation metrics were observed, demonstrating that longer-horizon forecasts are less robust.

Overall, these findings suggest that the developed processing chain can be applied reliably across different river systems; however, forecasts should be implemented with caution, and monitoring prediction variability, along with considering site-specific adjustments, is recommended when extending the model to new locations.

5.2 Operational Performance in the 2024-2025 ice season

The developed models were implemented in a near-real-time operational mode during the 2024–2025 river ice season. The system was launched upon the availability of new RCM imagery. SAR backscatter and PDD (derived from observed and forecasted temperatures) were used as input data to predict the likelihood of a breakup within a specific forecast window. The accuracy assessment of the issued forecasts is presented in Table 2, comparing the observed breakup dates with the predicted 50% probability dates.

The models demonstrated strong predictive performance, achieving mean absolute errors of 1.43 days for the two-week forecast and 2.14 days for the three-week forecast. The highest errors for the two-week model were observed in segment 4b, while the three-week model exhibited the largest errors in segments 6 and 2c.

Interestingly, both models achieved their best performance over segment 3c, despite this segment previously showing the lowest classification metrics during the model validation step. This may indicate that environmental conditions during the 2024-2025 season were more favorable in this segment.

Assessing the performance of the models over the Goose River, it is noteworthy that the three-week forecast at the second site was less accurate than the two-week forecast, consistent with our earlier evaluation results indicating that longer-term forecasts are generally less reliable.

Overall, the 2024-2025 season results were promising; however, further validation across additional seasons and sites is needed to confirm the model's reliability.

6. Discussion

RCM was launched in 2019, providing a relatively short temporal archive of only about four years of data available for this study. This limited time span constrains the amount of training data that can be used for ML applications, which are supposed to rely on large datasets to achieve high accuracy and generalization capability. Consequently, model performance may currently be affected by data scarcity. However, as RCM continues to acquire

Segment		2-week model				3 week - MODEL			
		MAE ± SD (Days)	OA	F1	Kappa	MAE ± SD (Days)	OA	F1	Kappa
Churchill River	2c	6.00 ± 4.74	0.920	0.921	0.839	4.25 ± 2.77	0.927	0.913	0.851
	3a	4.75 ± 3.90	0.948	0.949	0.896	6.00 ± 4.64	0.946	0.939	0.891
	3b	5.75 ± 3.63	0.953	0.952	0.906	6.50 ± 3.91	0.948	0.943	0.896
	3c	6.50 ± 5.59	0.899	0.889	0.796	6.25 ± 4.02	0.868	0.844	0.731
	4a	5.00 ± 2.12	0.914	0.899	0.823	5.52 ± 4.09	0.951	0.943	0.900
	4b	4.50 ± 2.29	0.899	0.914	0.796	7.25 ± 3.56	0.893	0.880	0.783
	6	8.75 ± 1.92	0.900	0.885	0.797	5.00 ± 3.94	0.906	0.878	0.802
Average		5.89 ± 3.46	0.919	0.916	0.836	5.82 ± 3.85	0.920	0.906	0.836
Goose River		5.50 ± 5.12	0.904	0.899	0.808	6.25 ± 3.49	0.827	0.743	0.616

Table 1. Leave-one-out cross-validation results

Segment		Observed Breakup Date	Two-week Model		Three-week Model	
			50% Probability Date	Δ (Days)	50% Probability Date	Δ (Days)
Churchill River	2c	2025-04-29	2025-05-01	-2	2025-05-03	-4
	3a	2025-05-01	2025-04-30	1	2025-05-03	-2
	3b	2025-05-05	2025-05-04	1	2025-05-04	1
	3c	2025-05-05	2025-05-05	0	2025-05-05	0
	4a	2025-05-07	2025-05-05	2	2025-05-05	2
	4b	2025-05-07	2025-05-04	3	2025-05-05	2
	6	2025-05-10	2025-05-09	1	2025-05-06	4
				MAE = 1.43		MAE = 2.14
Goose River		2025-05-05	2025-05-06	-1	2025-05-09	-4

Table 2. Model operational performance, 2024–2025 ice season

new observations in the coming years, the temporal record will expand substantially, reducing this limitation and enabling the development of more robust models.

Another major challenge arises from the heterogeneity of SAR data in general, and RCM in particular. RCM satellites operate in various beam modes, incidence angles, look directions, and spatial resolutions. Each of these acquisition parameters influences the backscatter signal. As a result, the same physical features may appear differently across images acquired under different acquisition settings. This variability introduces inconsistencies in the data distribution, which can degrade the performance of ML models.

Future research should focus on developing normalization and adaptation techniques that enable the effective integration of fused SAR data acquired from multiple satellites into machine learning models.

It is important to note that in this project, linear interpolation was employed to estimate the date at which the predicted probability of river ice breakup reached 50%. This approach was necessary due to the temporal resolution of the RCM data, which were acquired with a temporal resolution of approximately three to four days, with occasional gaps extending up to a week or longer. In reality, the transition from solid ice to open water is often abrupt rather than gradual, meaning that the probability of breakup does not increase smoothly over several days. Consequently, linear interpolation cannot capture the precise timing of the breakup event and introduces some uncertainty in the estimated dates. Future work should also focus on developing more robust evaluation strategies that account for both the abrupt nature of ice breakup and the temporal sparsity of SAR observations.

7. Conclusion

In this project, we focus on river ice breakup, which is defined as the moment when the area of open water starts to grow rapidly.

We developed a process linking SAR backscatter to the onset of river surface melt, which provided the opportunity for further development of an ML algorithm. This concept is based on the observation that increasing liquid water content within ice or snow leads to a decrease in SAR backscatter. Consequently, a time series of SAR backscatter observations can be used to detect the initiation of surface thaw, providing a basis for predicting the timing of upcoming river ice breakup.

A neural network MLP classifier was trained and evaluated using leave-one-out cross-validation, achieving an overall accuracy of 0.92, an F1-score of 0.91, and a Kappa coefficient of 0.84, with a MAE of 5.8 days. To our knowledge, this is the first model to directly incorporate SAR data as input into an ML framework for river ice breakup prediction.

The model was operationally implemented during the 2024-2025 river ice season, demonstrating strong performance, with MAE ranging from zero to four days across different river segments.

Furthermore, the approach was also tested on an independent site, over the western part of the Goose River. The models maintained strong predictive skill, achieving MAE of 5.5 and 6.25 days for the two-week and three-week forecasts, respectively. In near-real-time operational settings, the models predicted breakup with the MAE of approximately one and four days for the two-week and three-week forecasts.

Both the evaluation results during model development and the outcomes from the real-time operational implementation demonstrated strong predictive performance. However, we also acknowledge that the models were trained on a relatively limited dataset; therefore, the results should be interpreted with caution. Future work should focus on additional validation over other regions as well as further data collection to ensure the reliability and robustness of the approach.

8. Acknowledgements

The authors gratefully acknowledge financial support from Transport Canada through the National Trade Corridors Fund, as well as the NL Water Resources Management Division of the Department of Environment and Climate Change. This support made possible the development of the underlying concept as well as the implementation of the prediction models presented in this work.

9. References

Bamler, R., & Hartl, P. (1998). Synthetic aperture radar interferometry. *Inverse Problems*, *14*(4), R1. https://doi.org/10.1088/0266-5611/14/4/001

Beltaos, S. (2014). Hydrodynamic properties of ice-jam release waves in the Mackenzie Delta, Canada. *Cold Regions Science and Technology*, *103*, 91–106. https://doi.org/10.1016/j.coldregions.2014.03.011

Brangers, I., Lievens, H., Getirana, A., & De Lannoy, G. J. M. (2024). Sentinel-1 Snow Depth Assimilation to Improve River Discharge Estimates in the Western European Alps. *Water Resources Research*, *60*(11), e2023WR035019. https://doi.org/10.1029/2023WR035019

C-CORE. (2024). *Churchill River Ice Monitoring*. https://www.churchillriver.app/

Catchpole, A. J. W., & Moodie, D. W. (1974). Changes in the Canadian definitions of break-up and freeze-up. *Atmosphere*, *12*(4), 133–138. https://doi.org/10.1080/00046973.1974.9648379

CCCS. (2023). *ERA5 hourly data on single levels from 1940 to present*. ERA5 Hourly Data on Single Levels from 1940 to Present. Copernicus Climate Change Service (C3S) Climate Data Store (CDS). , DOI: 10.24381/Cds.Adbb2d47. https://cds.climate.copernicus.eu/datasets/reanalysis-era5-single-levels?tab=overview

CDSE. (2025, April 1). *Copernicus Data Space Ecosystem | Europe's eyes on Earth*. https://dataspace.copernicus.eu/

Chaouch, N., Temimi, M., Romanov, P., Cabrera, R., McKillop, G., & Khanbilvardi, R. (2014). An automated algorithm for river ice monitoring over the Susquehanna River using the MODIS data. *Hydrological Processes*, *28*(1), 62–73. https://doi.org/10.1002/hyp.9548

Department of Environment and Climate Change. (2025). *Water Resources—Dept. Of ECC - ADRSv6.0—List of Real Time Stations*. https://www.mae.gov.nl.ca/wrmd/ADRS/v6/Graphs_List.asp

ECC NL. (n.d.). *Churchill River Early Flood Warning and Alert System*. Department of Environment and Climate Change, Government of Newfoundland and Labrador, Canada. Retrieved November 1, 2024, from https://www.gov.nl.ca/ecc/waterres/flooding/lc-flood-warning/

Eckerstorfer, M., & Malnes, E. (2015). Manual detection of snow avalanche debris using high-resolution Radarsat-2 SAR images. *Cold Regions Science and Technology*, *120*, 205–218. https://doi.org/10.1016/j.coldregions.2015.08.016

Gädeke, A., Langer, M., Boike, J., Burke, E. J., Chang, J., Head, M., Reyer, C. P. O., Schaphoff, S., Thiery, W., & Thonicke, K. (2021). Climate change reduces winter overland travel across the Pan-Arctic even under low-end global warming scenarios. *Environmental Research Letters*, *16*(2), 024049. https://doi.org/10.1088/1748-9326/abdcf2

Hoppinen, Z., Palomaki, R. T., Brencher, G., Dunmire, D., Gagliano, E., Marziliano, A., Tarricone, J., & Marshall, H.-P. (2024). Evaluating snow depth retrievals from Sentinel-1 volume scattering over NASA SnowEx sites. *The Cryosphere*, *18*(11), 5407–5430. https://doi.org/10.5194/tc-18-5407-2024

Johnson, A., Fahnestock, M., & Hock, R. (2020). Evaluation of passive microwave melt detection methods on Antarctic Peninsula ice shelves using time series of Sentinel-1 SAR. *Remote Sensing of Environment*, *250*, 112044. https://doi.org/10.1016/j.rse.2020.112044

Jutila, A., & Haas, C. (2025). C and K band microwave penetration into snow on sea ice studied with off-the-shelf tank radars. *Annals of Glaciology*, *65*, e5. https://doi.org/10.1017/aog.2023.47

Landis, J. R., & Koch, G. G. (1977). The Measurement of Observer Agreement for Categorical Data. *Biometrics*, *33*(1), 159–174. https://doi.org/10.2307/2529310

Lee, J.-S. (1980). Digital Image Enhancement and Noise Filtering by Use of Local Statistics. *IEEE Transactions on Pattern Analysis and Machine Intelligence*, *PAMI-2*(2), 165–168. https://doi.org/10.1109/TPAMI.1980.4766994

Liston, G. E., & Hall, D. K. (1995). Sensitivity of lake freeze-up and break-up to climate change: A physically based modeling study. *Annals of Glaciology*, *21*, 387–393. https://doi.org/10.3189/S0260305500016116

Lund, J., Forster, R. R., Deeb, E. J., Liston, G. E., Skiles, S. M., & Marshall, H.-P. (2022). Interpreting Sentinel-1 SAR Backscatter Signals of Snowpack Surface Melt/Freeze,

Warming, and Ripening, through Field Measurements and Physically-Based SnowModel. *Remote Sensing*, *14*(16), Article 16. https://doi.org/10.3390/rs14164002

Lynch, M., Briggs, R., English, J., Khan, A. A., Khan, H., & Puestow, T. (2021). *Operational Monitoring of River Ice on the Churchill River, Labrador*. CGU HS Committee on River Ice Processes and the Environment.

Magnuson, J. J., Robertson, D. M., Benson, B. J., Wynne, R. H., Livingstone, D. M., Arai, T., Assel, R. A., Barry, R. G., Card, V., Kuusisto, E., Granin, N. G., Prowse, T. D., Stewart, K. M., & Vuglinski, V. S. (2000). Historical Trends in Lake and River Ice Cover in the Northern Hemisphere. *Science*, *289*(5485), 1743–1746. https://doi.org/10.1126/science.289.5485.1743

Muhammad, P., Duguay, C., & Kang, K.-K. (2016). Monitoring ice break-up on the Mackenzie River using MODIS data. *The Cryosphere*, *10*(2), 569–584. https://doi.org/10.5194/tc-10-569-2016

Mullan, D., Swindles, G., Patterson, T., Galloway, J., Macumber, A., Falck, H., Crossley, L., Chen, J., & Pisaric, M. (2017). Climate change and the long-term viability of the World's busiest heavy haul ice road. *Theoretical and Applied Climatology*, *129*(3), 1089–1108. https://doi.org/10.1007/s00704-016-1830-x

Natural Resources Canada. (n.d.-a). *Canadian Digital Elevation Model*. Retrieved October 16, 2024, from https://open.canada.ca/data/en/dataset/7f245e4d-76c2-4caa-951a-45d1d2051333

Natural Resources Canada. (n.d.-b). *Earth Observation Data Management System (EODMS)*. Retrieved October 16, 2024, from https://www.eodms-sgdot.nrcan-rncan.gc.ca/index-en.html

Ohmura, A. (2001). Physical Basis for the Temperature-Based Melt-Index Method. *Journal of Applied Meteorology and Climatology*, *40*(4), 753–761. https://doi.org/10.1175/1520-0450(2001)040%3C0753:PBFTTB%3E2.0.CO;2

Rokaya, P., Morales-Marin, L., & Lindenschmidt, K.-E. (2020). A physically-based modelling framework for operational forecasting of river ice breakup. *Advances in Water Resources*, *139*, 103554. https://doi.org/10.1016/j.advwatres.2020.103554

Scambos, T. A., Hulbe, C., Fahnestock, M., & Bohlander, J. (2000). The link between climate warming and break-up of ice shelves in the Antarctic Peninsula. *Journal of Glaciology*, *46*(154), 516–530. https://doi.org/10.3189/172756500781833043

Small, D., & Schubert, A. (2008). Guide to ASAR Geocoding. *RSL-ASAR-GC-AD*, (1.0).

Snapir, B., Momblanch, A., Jain, S. K., Waine, T. W., & Holman, I. P. (2019). A method for monthly mapping of wet and dry snow using Sentinel-1 and MODIS: Application to a Himalayan river basin. *International Journal of Applied Earth Observation and Geoinformation*, *74*, 222–230. https://doi.org/10.1016/j.jag.2018.09.011

Sobiech, J., & Dierking, W. (2013). Observing lake- and river-ice decay with SAR: Advantages and limitations of the unsupervised k -means classification approach. *Annals of Glaciology*, *54*(62), 65–72. https://doi.org/10.3189/2013AoG62A037

Solberg, R., Koren, H., Amlien, J., Malnes, E., Schuler, D. V., & Orthe, N. K. (2010). The development of new algorithms for remote sensing of snow conditions based on data from the catchment of Øvre Heimdalsvatn and the vicinity. *Hydrobiologia*, *642*(1), 35–46. https://doi.org/10.1007/s10750-010-0157-3

Tsai, Y.-L. S., Dietz, A., Oppelt, N., & Kuenzer, C. (2019). Remote Sensing of Snow Cover Using Spaceborne SAR: A Review. *Remote Sensing*, *11*(12), Article 12. https://doi.org/10.3390/rs11121456

USGS. (2025). *EarthExplorer*. https://earthexplorer.usgs.gov/

van der Sanden, J. J., Drouin, H., & Geldsetzer, T. (2021). An automated procedure to map breaking river ice with C-band HH SAR data. *Remote Sensing of Environment*, *252*, 112119. https://doi.org/10.1016/j.rse.2020.112119